

Article

The Influence of Environments on the Intensity Change of Typhoon Soudelor

Leo Oey^{1,2,*} and Yuchen Lin³¹ IHOS, National Central University, Taoyuan City 32001, Taiwan² AOS, Princeton University, Princeton, NJ 08544, USA³ CIGLR, University of Michigan, Ann Arbor, MI 48109, USA; lameixisi@gmail.com

* Correspondence: lyo@alumni.princeton.edu or lyoey@gmail.com

Abstract: Previous studies have shown that background oceanic and atmospheric environments can influence not only the formation but also the intensity of tropical cyclones. Typhoon Soudelor in August 2015 is notable in that it underwent two rapid intensifications as the storm passed over the Philippine Sea where the 26 °C isotherm (Z_{26}) was deeper than 100 m and warm eddies abounded. At the same time, prior to the storm's arrival, an anomalous upper-level anticyclone developed south of Japan and created a weakened vertical wind shear (V_s) environment that extended into the Philippine Sea. This study examines how the rapid intensification of Typhoon Soudelor may be related to the observed variations of Z_{26} , V_s and other environmental fields as the storm crossed over them. A regression analysis indicates that the contribution to Soudelor's intensity variation from V_s is the largest (62%), followed by Z_{26} (27%) and others. Further analyses using composites then indicate that the weak vertical wind shear produced by the aforementioned anomalous anticyclone is a robust feature in the western North Pacific during the developing summer of strong El Ninos with Oceanic Nino Index (ONI) > 1.5.



Citation: Oey, L.; Lin, Y. The Influence of Environments on the Intensity Change of Typhoon Soudelor. *Atmosphere* **2021**, *12*, 162. <https://doi.org/10.3390/atmos12020162>

Keywords: typhoon rapid intensification; tropical cyclones; vertical wind shear; upper-ocean warm eddies; 26 °C isotherm; El Nino; western North Pacific; upper-tropospheric anticyclone; Philippine Sea

Academic Editors:

Sundararaman Gopalakrishnan and Ghassan Alaka

Received: 31 December 2020

Accepted: 23 January 2021

Published: 27 January 2021

Publisher's Note: MDPI stays neutral with regard to jurisdictional claims in published maps and institutional affiliations.



Copyright: © 2021 by the authors. Licensee MDPI, Basel, Switzerland. This article is an open access article distributed under the terms and conditions of the Creative Commons Attribution (CC BY) license (<https://creativecommons.org/licenses/by/4.0/>).

1. Introduction

It is well documented that large-scale environmental conditions exert strong controls upon tropical cyclone formation [1]. In addition to the three favorable conditions of cyclonic low-level wind vorticity, high humidity and maximum potential intensity (MPI) [2,3], tropical cyclones tend to form also in regions where the vertical wind shear is not strong ($V_s = |V_{200\text{hPa}} - V_{850\text{hPa}}| \lesssim 10$ m/s, where V is the wind vector) and the depth of the ocean's 26 °C isotherm is sufficiently deep ($Z_{26} \gtrsim 60$ m) [1,4]. In the western North Pacific, favorable climatological summer conditions of these environmental parameters, the first three in particular, generally overlap in a fairly large region, roughly in longitudes 120~160° and latitudes 8~23° N [5]. The region encompasses the "doldrum equatorial trough" or "monsoon trough", where the high-humidity south-southwesterly wind converges with the easterly trade wind [5].

Studies have found also that V_s and Z_{26} are in some cases statistically correlated with tropical cyclone intensity change [6–15]. The correlation appears to be related to the changing V_s and/or Z_{26} field that the storm experiences as it translates through these fields. Examples are [8] for tropical cyclones Gwenda (1999) and Rewa (1993) as the storms move through their respective environmental V_s field, and [10] for Hurricane Katrina (2005) in the Gulf of Mexico, as the Z_{26} changes when the storm crosses the Loop Current and associated mesoscale eddy field. Although the environmental V_s and Z_{26} fields can evolve, the evolution is in most cases sufficiently slow compared to the time scale of the translating storm that they may be assumed to be approximately frozen at the state prior to the storm's

arrival. Therefore, the changes in V_s and Z_{26} are primarily because the storm experiences different environments along its track as it translates across these fields.

This study examines how the V_s , Z_{26} and other environmental parameters may be related to the intensity change of Typhoon Soudelor in August 2015 in the Philippine Sea (see Figure 1). Typhoon Soudelor was the strongest tropical cyclone of the 2015 western North Pacific typhoon season. A lifetime maximum one-minute sustained wind speed of 79 m/s was recorded by the Joint Typhoon Warning Center (JTWC). The typhoon caused 40 known fatalities, extensive floods and extended power outages as it made landfall across Taiwan and southeastern China. The storm underwent two rapid intensifications over the Philippine Sea east of Luzon, where warm eddies with deep $Z_{26} \gtrsim 100$ m abounded [16–18]. A number of case studies have suggested that warm eddies with deep Z_{26} may trigger the intensification and rapid intensification of typhoons in the western North Pacific (for example, see [7]). Less systematic case studies have been conducted on the roles of other environmental parameters, for example, the vertical wind shear. Here we use observations to estimate the potential influence of Z_{26} and V_s , as well as other parameters, on the intensity change of Typhoon Soudelor. We find that Soudelor's intensity change is related more to V_s than Z_{26} and other parameters. This is due to the presence of a small area—a “pocket”, roughly $1500 \text{ km} \times 1500 \text{ km}$, of very weak environmental wind shear ($V_s < 4 \text{ m/s}$) south of Japan and into the central Philippine Sea, which the storm crossed. The result suggests that small pockets of vertical wind shear field embedded in the aforementioned favorable climatology in the western North Pacific in (cyclonic low-level wind vorticity, high humidity and MPI) may have influenced the rapid intensification of Soudelor and also may play a role in the intensity change of other typhoons. A further analysis indicates that the low- V_s pocket is a consistent feature of the atmospheric conditions in the western North Pacific in the summer, preceding a strong El Niño.

2. Data and Methods

2.1. Data Sources

Typhoon Soudelor's six-hourly track locations and corresponding maximum wind speed (V_{\max}) were based on the averages of data from the JTWC and the Japan Meteorological Agency (JMA), obtained from the International Best Track Archive for Climate Stewardship (IBTrACS) database. Before averaging, the JTWC 1-min wind was multiplied by a factor of 0.88 to make it consistent with the JMA 10-min wind definition. The Z_{26} was calculated using version 4.2.1 of the Meteorological Office Hadley Center (the EN4) ocean reanalysis dataset [19], which provides monthly sea-surface temperature as well as vertical profiles of temperature on a $1^\circ \times 1^\circ$ grid, based on objective analysis of all types of ocean profiling instruments, for example, the Argo float. The locations of eddies inferred from the EN4's Z_{26} field were verified using the $1/4^\circ \times 1/4^\circ$ gridded sea surface height from satellite altimetry observations and the $0.1^\circ \times 0.1^\circ$ gridded sea surface temperature (SST) data from the Group for High Resolution Sea Surface Temperature (GHRSSST). Atmospheric climatological fields such as the vertical wind shear, humidity, etc., were calculated using the monthly National Centers for Environmental Prediction (NCEP) reanalysis data on a $1^\circ \times 1^\circ$ grid.

2.2. Along-Track Environmental Values

All environmental parameters were calculated using fields prior to Typhoon Soudelor on 1 August 2015 UTC and are assumed fixed throughout the period of the storm. Thus, as explained in the Introduction, the environmental fields varied along the track of the storm purely due to its translation. For Typhoon Soudelor, the translation speed was approximately 450–500 km/day. Along-track, six-hourly environmental values were then obtained by averaging the corresponding field over a circular area of 150 km radius, centered about the track locations. For the vertical wind shear, this is the same as the “method 1” specified in [8]. Averaging yields smoother series. However, the result is not overly sensitive to the averaging area, even when values at the track points were directly

used without averaging. Note that as monthly fields prior to Typhoon Soudelor were used, we treated them as already representing the large-scale environmental conditions unaffected by the storm, and therefore did not apply any special treatments. For example, for V_s , we did not average in the annulus region between 200 and 800 km radii from the typhoon center as is commonly done (for example, see [20]).

2.3. A Regression Model to Assess the Environmental Contributions to Intensity Change

To estimate the contributions of various environmental parameters to the intensity change of Typhoon Soudelor, we used a diagnostic index called the Intensity Change Index ICI [13]. The ICI is fashioned after the Genesis Potential Index widely used in the literature to diagnose the formation of tropical cyclones [21,22]:

$$ICI = \left(\frac{RH}{50}\right)^{0.8} \left(\frac{MMPI}{70}\right)^{3.2} (1 + 0.1 \times V_s)^{-1.6}. \quad (1)$$

where RH is the 600 hPa relative humidity, V_s is the vertical wind shear defined previously, and $MMPI$ is a modified maximum potential intensity in which the SST in the MPI formula is replaced by T_{mix} , a temperature averaged from the sea surface to a depth h_{mix} below the surface [23]. The rationale is that, due to mixing of warm surface with cool subsurface waters by the tropical cyclone wind, the SST is cooled, and the degree of cooling depends on how deep the upper-ocean warm layer is in the vicinity of the storm's eye. To calculate T_{mix} , we assumed that the temperature profile was linear between the surface and the 26 °C isotherm (Z_{26}), and then depth-averaged the profile over h_{mix} , yielding

$$T_{mix} = SST - [(SST - 26) h_{mix} / (2Z_{26})] H_v(SST - 26), \quad (2)$$

where $H_v(\phi) = 1$ for the value of the argument $\phi > 0$, $= 0$ for $\phi \leq 0$, as the Heaviside function, and SST and Z_{26} are taken from their pre-storm observed values, described previously. Equation (2) indicates that, because of wind mixing, T_{mix} is cooler than the pre-storm SST, and the cooling is more in regions where Z_{26} is thin, and is less where Z_{26} is thick. Strictly speaking, h_{mix} should be a function of the wind speed (and other parameters, such as stratification), but for simplicity we set $h_{mix} = 50$ m [23].

Knowing the SST and Z_{26} , as well as the atmospheric profiles of temperature, pressure, specific humidity, etc., from observations, the $MMPI$ can be calculated by modifying the code for MPI [3]. The ICI can then be calculated by inputting the observed RH and V_s in Equation (1). If ICI can provide a measure of intensity, the formula then indicates that Typhoon Soudelor's intensity strengthens, in other words, the change in ICI : δICI is positive as the storm moves into a region of decreased V_s and/or increased RH and $MMPI$. On the other hand, as Soudelor's intensity weakens, δICI is negative as the storm moves into a region of increased V_s and/or decreased RH and $MMPI$. Note that the influence of Z_{26} and/or SST on intensity change is implicit in $MMPI$. In the study region where Soudelor underwent its strongest intensification, east from the Luzon-Mindanao island chain to the central tropical Pacific, the summertime SST as well as the atmospheric profiles varied little. The $\delta MMPI$ was mainly controlled by δZ_{26} , whose scale depends on smaller oceanic mesoscale eddies, about 200 km~500 km [18].

Instead of the ICI , other similar formulae may be used, for example, the Genesis Potential Index (though strictly speaking it has only been applied to assess "tropical cyclone genesis"). The ICI suffices for the present study, however, and is convenient since the coefficients (0.8, 3.2 and -1.6 in Equation (1)) have already been previously calculated using observations, to optimize the correlation between δICI and intensity change in the Philippine Sea [13]. To estimate the contributions of V_s , RH and $MMPI$ to the intensity change of Typhoon Soudelor, we first checked the formula by regressing ICI against the observed maximum wind speed, V_{max} . We repeated the calculation setting each of V_s , RH and $MMPI$ as fixed, and assessed their separate contributions. These are presented in Section 3.

3. Results

This section describes the environmental conditions during the formation (Section 3.1), intensification (Section 3.2) and weakening (Section 3.3) phases of Typhoon Soudelor. Section 3.4 then uses the data and method described in Section 2 to estimate the contributions of various environmental parameters to the intensity change of Typhoon Soudelor. Section 3.5 describes how a low- V_s pocket south of Japan developed in the Summer 2015, and compares it with other El Nino summers.

3.1. Environment during Formation (30 July 2015)

Figure 1 shows Typhoon Soudelor's track with daily locations marked by circles, color-filled according to the storm's intensity. Soudelor formed on 30 July UTC (all times specified herein are UTC) as a tropical depression near $162^\circ, 14^\circ$ N. The background vectors and shading are 1000-hPa wind and divergence. Soudelor's genesis location is near the eastern convergence zone of the "doldrum equatorial trough" [5], where the southerly and southwesterly surface wind converged with the easterly trade wind, and the wind was weak.

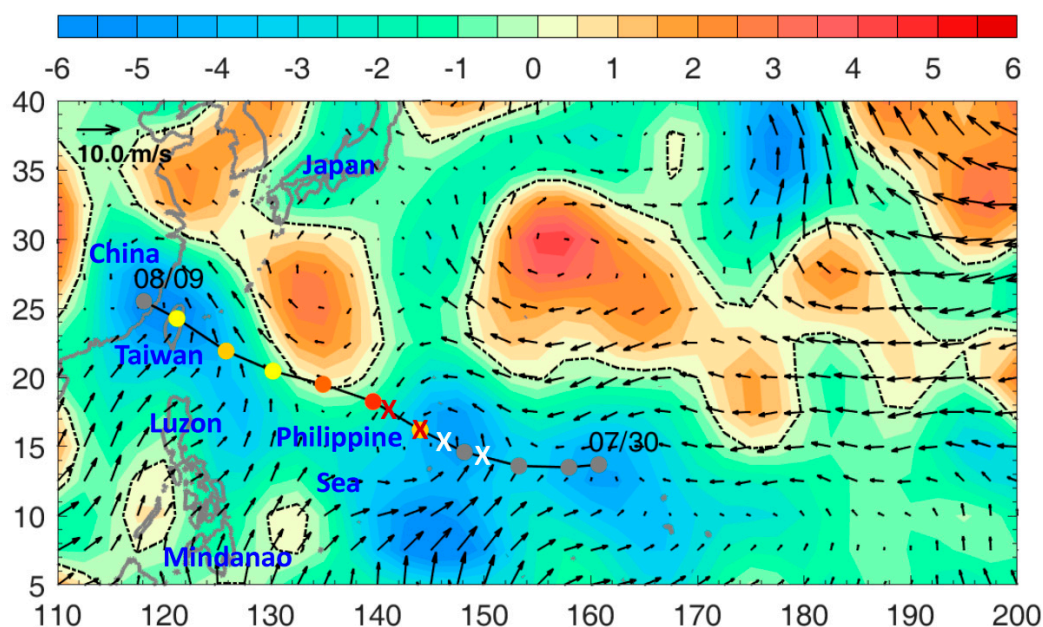


Figure 1. Typhoon Soudelor track (line with filled circles) and daily locations from formation on 30 July 2015 UTC to dissipation on 9 August 2015 UTC when the storm crossed southeastern China. Track locations are colored using the Saffir-Simpson scale: grey = tropical storm and (yellow, gold, orange, deep-orange, red) = Categories (1, 2, 3, 4, 5), respectively, based on the observed (1-min) maximum wind speed. The pairs of white and red "X" mark the beginning and end points of rapid-intensification events RI1 and RI2 (see text). Vectors and shading are pre-Soudelor (1 August 2015 UTC) 1000 hPa wind $V_{1000\text{hPa}}$ (m/s), and divergence $\nabla \cdot V_{1000\text{hPa}}$ (10^{-6} s^{-1}), calculated from the NCEP reanalysis data. The map's x -axis is longitude from 110° to 200° , and y -axis is latitude from 5° N to 40° N. This plot also serves as a locator map, with location names indicated as referred to in the text. The Philippine Sea is bordered by the island chain from Mindanao, Taiwan to Japan in the west and north, the Mariana Islands in the east ($\sim 155^\circ$), and the Indonesian Archipelago ($\sim 2^\circ$ N) in the south.

Figure 2 shows the vertical wind shear. Since the upper-tropospheric flow is generally much stronger than the near-surface wind, the pattern of $V_s = |V_{200\text{hPa}} - V_{850\text{hPa}}|$ is mainly controlled by $V_{200\text{hPa}}$. The zonal belt of weak wind shear, $V_s < 4 \text{ m/s}$, seen in the figure (east of 155° and between 10° N and 14° N) aligns well with the Intertropical Convergence Zone (ITCZ), which lies between 10° N– 14° N in the Pacific in boreal summer

and zonally extends westward off the South American coast to about 155° . Above the ITCZ, the $|V_{200\text{hPa}}|$, hence the V_s , is weak. Soudelor's genesis location is near the western edge of this zonal belt of weak wind shear.

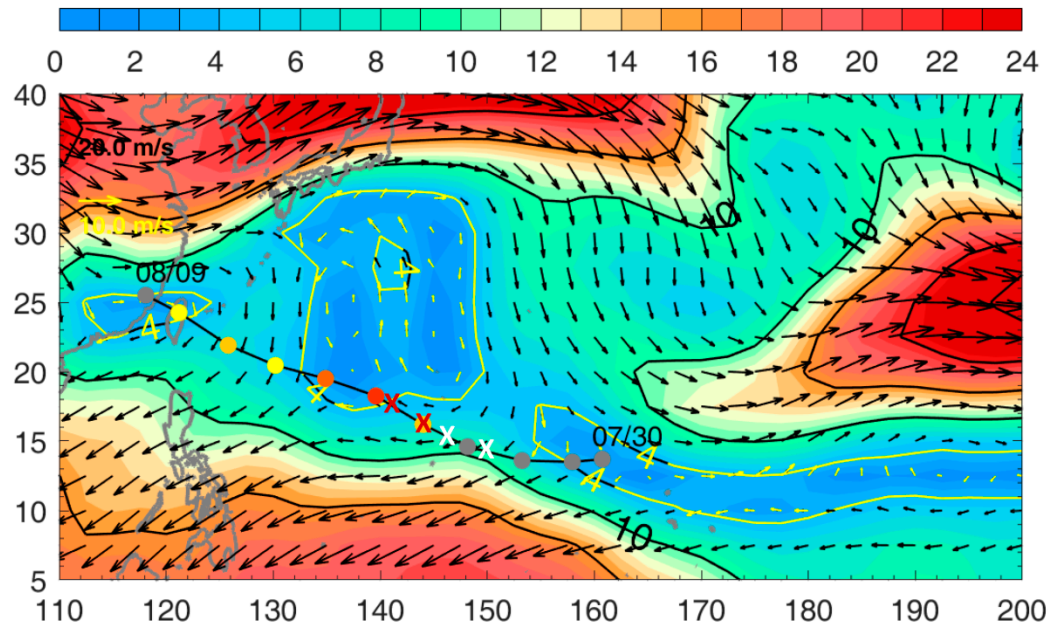


Figure 2. Pre-Typhoon Soudelor (1 August 2015 UTC) vertical wind shear, $V_{200\text{hPa}} - V_{850\text{hPa}}$, and magnitude, $V_s = |V_{200\text{hPa}} - V_{850\text{hPa}}|$, $V =$ wind velocity: vectors and color shading with contours = 4, 10, 16, etc., m s^{-1} , the 4 m/s contour is highlighted in yellow, calculated from the NCEP reanalysis data. See Figure 1 notes for the typhoon track and other plot information.

Figure 3 shows the 26°C isotherm. A zonal belt of warm eddies, closed contours of deepened $Z_{26} > 100\text{ m}$ between 12°N – 18°N in the Philippine Sea, can be seen to populate the region, east from the coast of Luzon to about the 170° . This eddy belt is actually embedded on top of a semi-permanent, climatological Z_{26} ridge (where $Z_{26} \gtrsim 80\text{--}90\text{ m}$) caused in part by the presence of subsurface “mode water” in the main thermocline north of the ridge [24]. Soudelor's genesis location is near the eastern end of the eddy belt. Moreover, the July–August SST over the broad tropics (including the Z_{26} ridge) reaches as high as 30°C . These combined favorable environmental conditions of warm SST, deep Z_{26} , surface wind convergence, and weak vertical wind shear likely contributed to the formation of Typhoon Soudelor on 30 July 2015 near $162^\circ, 14^\circ\text{N}$.

3.2. Environment during Intensification (Aug/01/00:00 to Aug/03/18:00)

Typhoon Soudelor continued to intensify during the next two days (30 July to 1 August) as the storm moved west-northwestward, driven in part by the steering wind of the North Pacific Subtropical High (for example see [25]). It became a tropical storm on 1 August 2015. Figure 4 (black line) shows the intensity evolution of Typhoon Soudelor from 1 to 8 August (when the storm crossed Taiwan). The corresponding V_s and Z_{26} are plotted as green and blue lines.

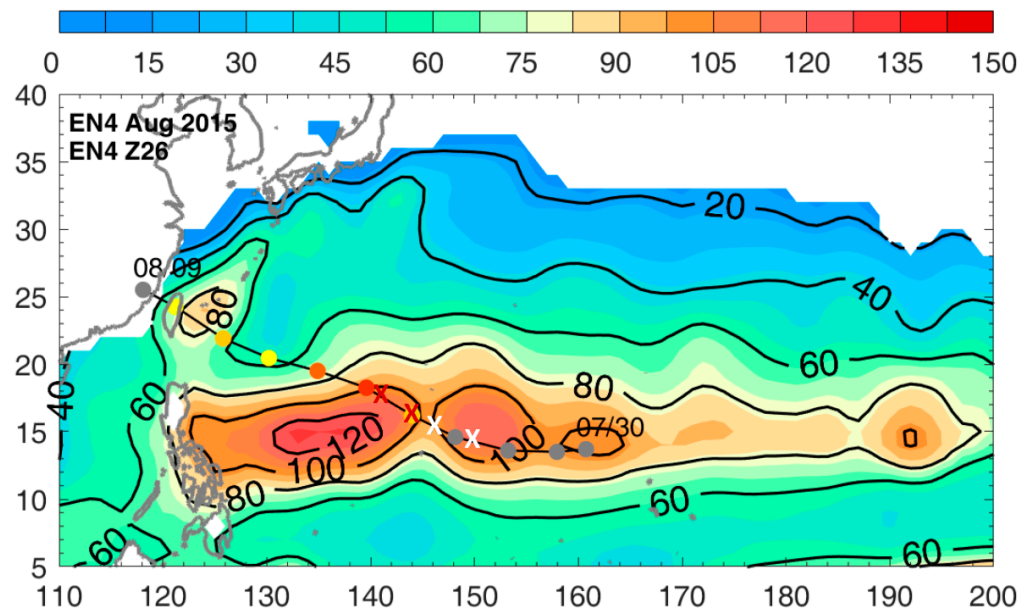


Figure 3. Pre-Soudelor (1 August 2015 UTC) Z_{26} (m; color shading and contours) calculated from the EN4 data. See Figure 1 notes for the typhoon track and other plot information.

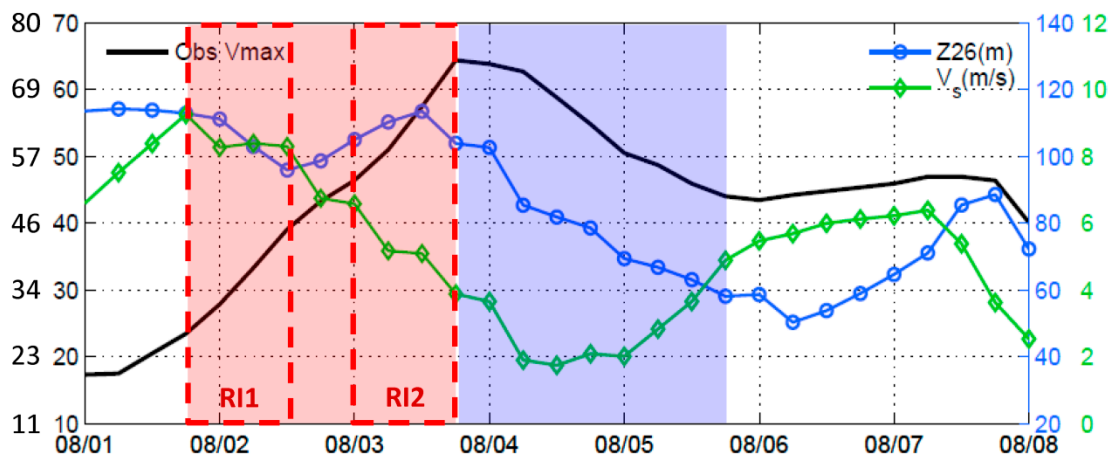


Figure 4. Typhoon Soudelor’s along-track time series from 1 to 8 August 2015 of V_{max} (black m/s; left ordinate) and V_s and Z_{26} (green m/s and blue m, respectively; right ordinate). Red dashed boxes enclose the two rapid intensification events, RI1 and RI2 (see text). Red and blue shadings indicate the 2-day intensification and 2-day weakening periods, respectively, analyzed in Section 3.4. The V_{max} here is 10-min maximum wind speed based on the average of JTWC and JMA, in which the JTWC 1-min wind was first reduced by a factor of 0.88 to make it consistent with the JMA 10-min wind definition. For reference, the outer scale of V_{max} (left ordinate) gives the approximate 1-min wind.

From Aug/01/18:00 to Aug/02/12:00 (red dashed box #1 in Figure 4), Soudelor underwent its first rapid intensification (period RI1). The maximum 1-min wind speed increased from 26 to 45 m/s in an 18-h period, according to the JTWC data, exceeding the rapid intensification criterion that the maximum 1-min wind speed increases by 15.4 m/s in a 24-h period [26]. The RI1 period is indicated by the two white crosses “X” in Figures 1–3. During the RI1, the V_s decreased slightly but remained above 8 m/s, while the Z_{26} remained deeper than ~100 m, though it decreased slightly as the storm was leaving a warm eddy (Figure 3).

After a brief 12-h period from Aug/02/12:00 to Aug/03/00:00, when Soudelor’s intensification rate slowed slightly as the storm underwent an eyewall replacement cycle, the storm underwent its second rapid intensification (period RI2; red “X” in Figures 1–3

and second red dashed box in Figure 4) from Aug/03/00:00 to Aug/03/18:00 and exploded into a Category-5 super-typhoon. The JTWC 1-min maximum wind speed recorded an increase from 52 to 79 m/s during this 18-h period (the JMA equivalent 1-min peak speed on Aug/03/18:00 was less ≈ 70 m/s, resulting in an average of about 75 m/s; see Figure 4). In contrast to the slight V_s variation during RI1, the V_s during RI2 rapidly decreased as Soudelor entered a “pocket” of low $V_s < 4$ m/s that extended from the south coast of Japan to the central Philippine Sea (about 20° N). Moreover, the Z_{26} remained deep and was actually deepening as Soudelor entered a second warm eddy (Figure 3).

3.3. Environment during Weakening (Aug/03/18:00 to Aug/08/00:00)

Typhoon Soudelor weakened rapidly after RI2, from Aug/03/18:00 to 6 August, coinciding with the time when Z_{26} shallowed as the typhoon left a warm eddy. At the same time, V_s increased as the storm left the low- V_s pocket. From 6 to 8 August, Soudelor strengthened prior to landfall across Taiwan, coinciding with the storm crossing over a region of slightly deepened Z_{26} , caused by the warm Kuroshio water east of Taiwan [16]. At the same time, V_s varied little, except in the last 12 h prior to landfall. Throughout the entire weakening phase from Aug/03/18:00 to 8 August, V_s remained low (< 7 m/s) and Soudelor’s intensity was well-correlated with Z_{26} (Figure 4; the correlation coefficient = 0.92, p -value < 0.01). The lower Z_{26} from Aug/03/18:00 to 6 August may be related to the existence of cold eddies [27].

3.4. Estimation of the Contributions of Environmental Parameters to Soudelor’s Intensification and Weakening

We used the ICI to assess the relative contributions of V_s , $MMPI$ (Z_{26}) and RH to Soudelor’s intensity variation, focusing on the rapid intensification and rapid weakening periods from Aug/01/18:00 to Aug/05/18:00 (see Figure 4, red and blue shaded regions). To do this, we first verified that the ICI could serve as a proxy of the environmental influence on intensity, by regressing the observed V_{max} against the ICI , as shown in Figure 5a. The regression was done by first removing the mean, then dividing by the standard deviation of each variable, and finally plotting with the intercept removed for plot clarity. The r^2 and p -value were unchanged by the procedure [28]. The ICI explained 83% of V_{max} -variance and was highly significant with a regression slope ($=0.91$) close to one. We should emphasize that this regression deteriorated if the three power coefficients ($=0.8, 3.2, -1.6$) in Equation (1) were changed [13]. Thus the ICI was a reasonably good proxy of V_{max} during the rapid intensification and rapid weakening phases of typhoon Soudelor.

We could now estimate the contribution of each of the above three parameters on intensity by repeating the regression calculation, but keeping in turn each parameter fixed at its respective mean value. The results are shown in Figure 5b–d. The percentage variance explained decreases to 71% when RH was kept fixed (Figure 5b), to 54% when $MMPI$ was kept fixed (Figure 5c) and to an insignificant 18% when V_s was fixed (Figure 5d). In the last case, with V_s fixed, the ICI failed to serve as a useful proxy of V_{max} . Indeed, the percentages of the V_{max} -variance contributed by RH , $MMPI$, and V_s were 11%, 27%, and 62%, respectively, indicating the predominant control of the vertical wind shear to the intensity variation of Soudelor. As explained previously, the $MMPI$ variation was mainly contributed by Z_{26} , and the percentage of the V_{max} -variance explained by Z_{26} was bounded by that of $MMPI$ ($=27\%$). The RH had the least effect on V_{max} , contributing only 11% to the V_{max} -variance. This is because RH varies little in the Philippine Sea east of Luzon, and also among the three power coefficients in Equation (1), that of RH ($=0.8$) was the smallest, indicating the least sensitivity.

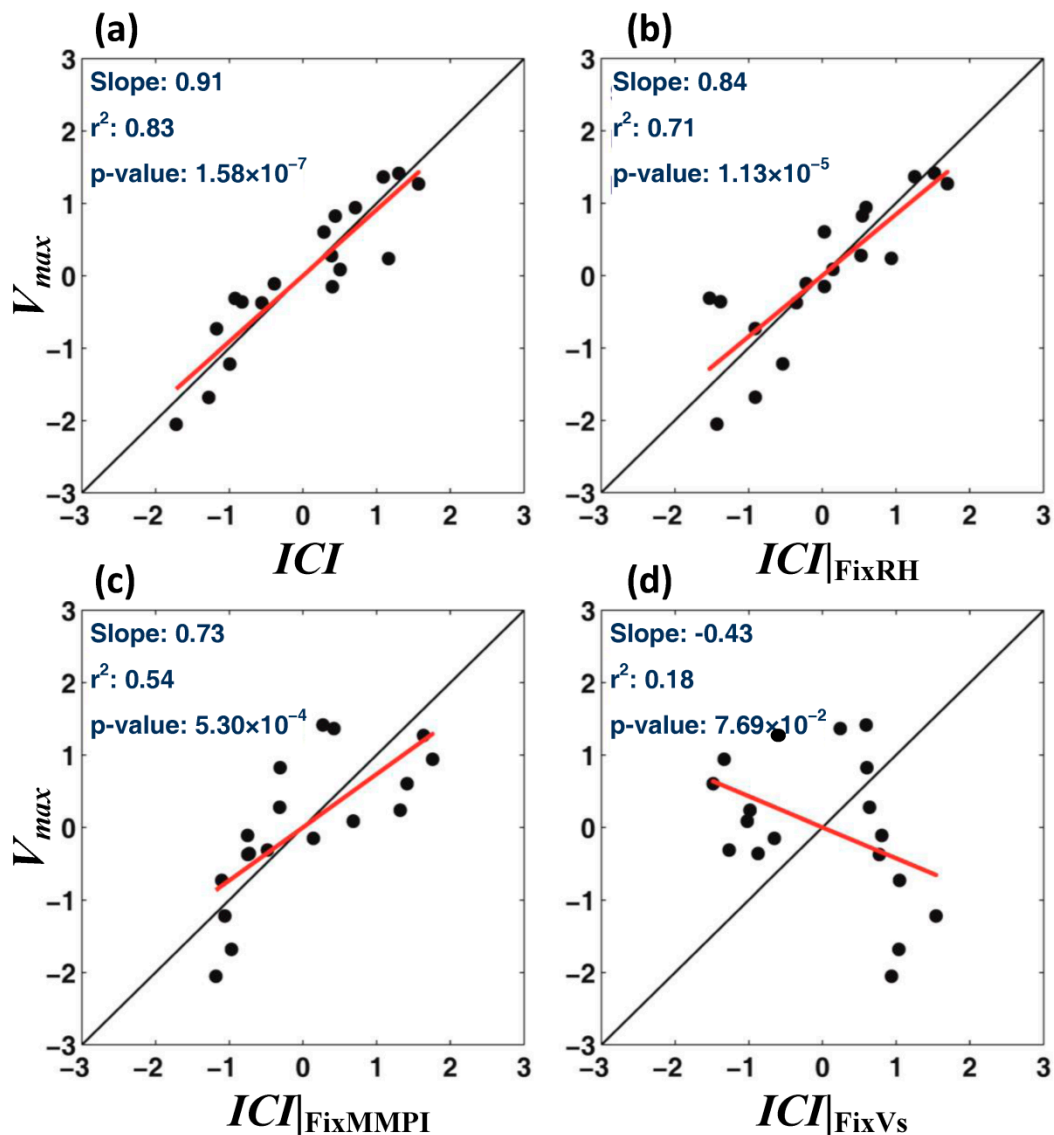


Figure 5. Regressing Soudelor V_{max} against (a) ICI ; (b) ICI with RH kept fixed; (c) ICI with $MMPI$ kept fixed; (d) ICI with V_s kept fixed. The analysis period was Aug/01/18:00 to Aug/05/18:00. Black dots are data points; red line is the regression with legends showing the corresponding slope, r^2 , and p ; black 45° line is for reference only. See text for further information.

3.5. The Low $V_s < 4$ m/s Pocket South of Japan

The above results suggest that the dependence of Soudelor's intensity on V_s during the rapid intensification and weakening phases is in part related to the storm entering and leaving the pocket of low $V_s < 4$ m/s over the Philippine Sea (Figure 2). The dependency is consistent with previous studies that show that $V_s \gtrsim 10$ m/s is detrimental to tropical cyclone intensification [29], $V_s < 10$ m/s favors intensification and, in particular, $V_s \lesssim 4$ m/s favors rapid intensification [8]. In the case of Soudelor, the storm rapidly intensified as it was entering the low pocket of $V_s < 4$ m/s, and rapidly weakened as it was leaving. To see how the anomalous low- V_s pocket arose in the case of Soudelor, we compared the climatological winds at 200 hPa and 850 hPa, and their difference, V_s (Figure 6), with the corresponding winds in Summer 2015 (Figure 7).

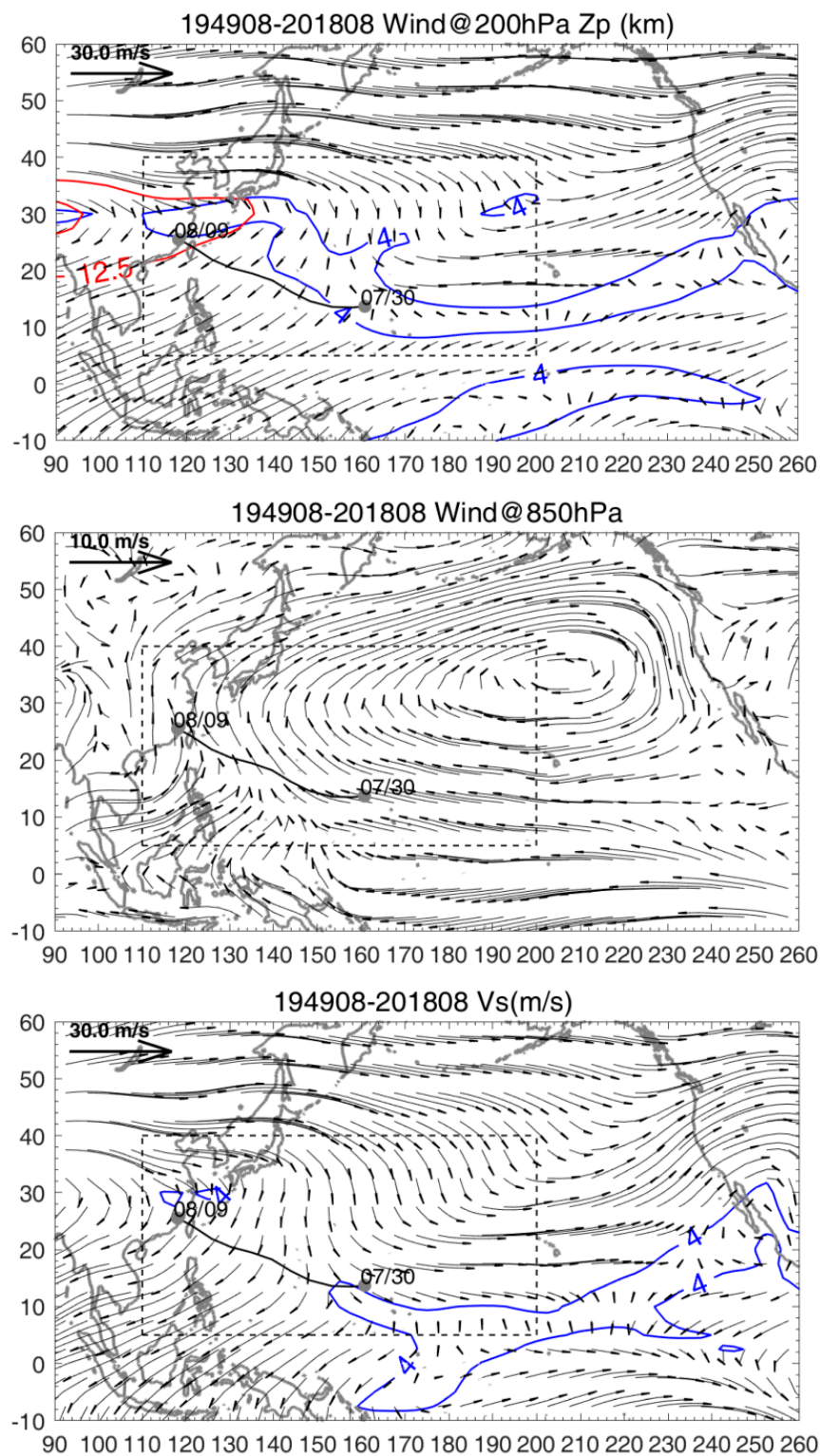


Figure 6. Mean (1948–2018, 1 August) climatological winds at 200 hPa (top) and 850 hPa (middle), and their difference, V_s (bottom). Red contours in top show $Z_p = 12.5$ and 12.55 km and blue contours in top and bottom show the 4 m/s wind. Typhoon Soudelor track is shown for reference in the study area (dashed rectangle).

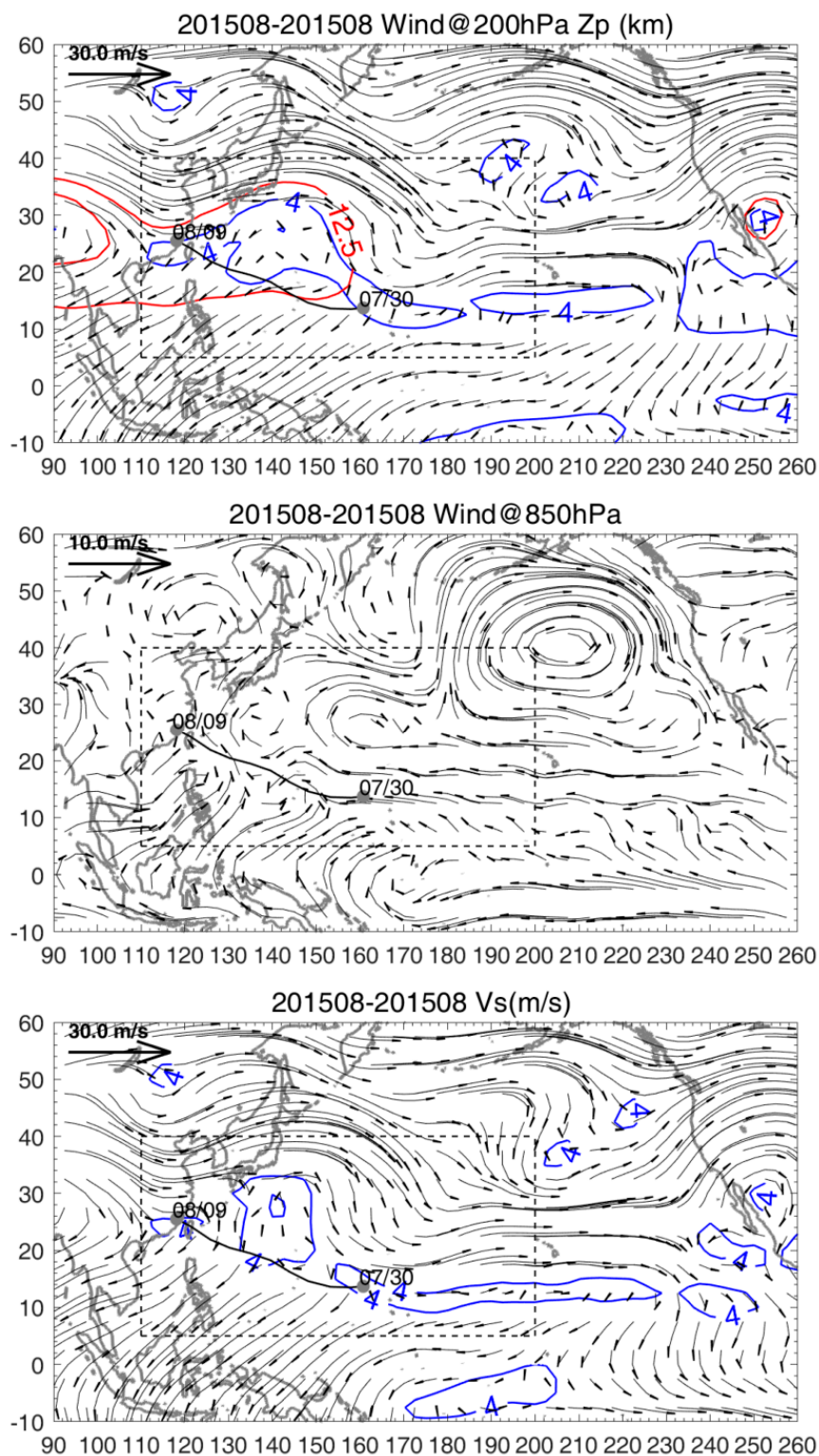


Figure 7. Same as Figure 6 but for pre-Soudelor (1 August 2015 UTC) environmental winds.

The climatological wind at 200 hPa (Figure 6 top) displays a mid-latitude wave pattern that has been extensively studied: a high over Tibet (90° , 30° N; see the red geopotential height contours), a broad trough over the ocean (180° – 210° , 30° N), and another high over Mexico (255° , 25° N), due to land-ocean heating and thermal contrasts [30,31]. In the study region (dashed rectangle), the westerly flow turns smoothly clockwise downstream of the Tibet high. South of Japan, the westerly wind becomes a weak northerly as the flow loops back in a clockwise turn to become easterly over the south-central Philippine Sea. Near the surface (@850 hPa, Figure 6 middle), the study region is under the western influence of the North Pacific Subtropical High, and the climatological wind is southerly. South of Japan, while both 200 and 850 hPa winds are weak, they are oppositely directed, and the difference, V_s , becomes quite significant, >4 m/s (Figure 6 bottom).

By contrast, in Summer 2015, the 200 hPa mid-latitude wave displays a strong meander immediately downstream of the Tibet high, as a secondary high now appears south of Japan, and the two highs sandwich a cyclonic meander in between (Figure 7 top; see red geopotential height contours). The effect of the secondary high also penetrates to 850 hPa, where one can see a weak circulation pattern of the same anticyclonic sign as at 200 hPa south of Japan (Figure 7 middle). Therefore, a weak wind shear “pocket”, $V_s < 4$ m/s, is produced from south of Japan to the central Philippine Sea (Figure 7 bottom, blue contour).

The secondary high anomaly south of Japan and the corresponding low- V_s pocket, developed during Summer 2015, of a very strong El Niño: the 2015/2016 El Niño (its Oceanic Niño Index (ONI) exceeded 2.5) [32]. We sought to discover whether the anomaly developed in 2015 only, or if it was a more robust feature of the developing summer of an El Niño year (“El Niño summer”). We defined the anomaly of a physical variable as “variable minus its climatology” and calculated composites of the anomalies of geopotential height and wind fields for different El Niños. We found a consistent pattern for strong El Niños with ONI > 1.5 after (and including) the 1965/1966 El Niño: 1965, 1972, 1982, 1987, 1991, 1997, 2009 and 2015. Figure 8 shows the anomalies of the 200 hPa minus 850 hPa geopotential height and wind for 2015 (Figure 8a) and El Niño composite (Figure 8b). Note that while the geopotential height difference is used, it is dominated by the values at 200 hPa. The secondary high south of Japan appears in both the 2015 and the El Niño composite plots as a positive anomaly extending from the central-eastern tropical Pacific where SST warming develops during an El Niño summer. South of Japan, the anomalous wind shear vector is southerly acting to weaken the northerly wind shear there, as discussed previously. The weakened wind shear can be seen as the low V_s pocket enclosed by the blue contour in each plot. Due to the averaging, the weakest composite mean wind shear exceeds 4 m/s (~ 4.5 m/s), and the 5 m/s contour is used in Figure 8b to indicate the low V_s pocket. Although not shown in Figure 8, a composite of moderate–strong La Niña (ONI < -1 : 1955, 1970, 1973, 1975, 1988, 1995, 1998, 1999, 2007, 2010 and 2011) yields a nearly reversed pattern: a negative geopotential height anomaly south of Japan, as well as a northerly V_s anomaly that strengthens the wind shear, so that $V_s \approx 8$ m/s or greater nearly everywhere over the western North Pacific.

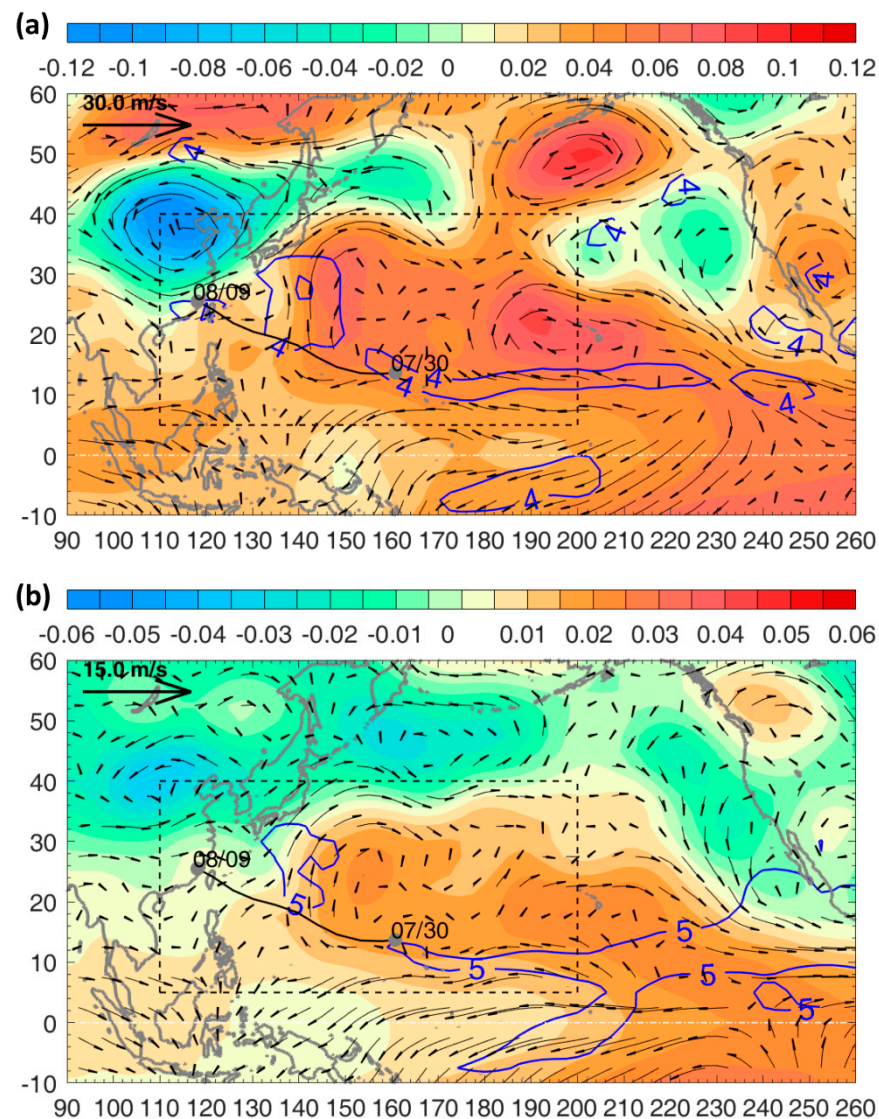


Figure 8. August 1 geopotential height difference (km, shading) and wind shear (m/s, vectors) anomalies for (a) 2015, and (b) El Niño (ONI > 1.5) composite: 1965, 1972, 1982, 1987, 1991, 1997, 2009, 2015; 90% significance $|$ values $|$ are > 0.013 km and 2 m/s. Blue contours are total (not anomaly) wind shear values of 4 m/s and 5 m/s, chosen to represent the low V_s in the 2015 and composite plots (see text). Typhoon Soudelor track is shown for reference in the study area (dashed rectangle).

4. Discussion

Wen et al. [33] conducted composite analyses to study East Asian rainfall during El Niño summers. El Niños of all intensities with ONI > 0.5 were studied, but distinction was made between Eastern Pacific and Central Pacific types, whereas in the present study only strong El Niños (ONI > 1.5) were used without differentiating the types. (According to Wen et al.'s classification, five of the eight El Niños chosen in our study are of the Eastern Pacific type, while the remaining three are of the “mixed” type). Nonetheless, despite these differences and other details, as well as the different goals of the two studies, the 200 hPa geopotential height composite shown in Wen et al.'s Figure 2 has a number of striking similarities with the composite of Figure 8 in this study. Both display a pair of warm patterns of amplitude 10~20 m straddling the equatorial Pacific, which Wen et al. attributed as the Matsuno-Gill's Rossby wave pair in response to tropical heating [34,35]. Both also display (circum-global) low pressure belt and wave train at mid-latitude 30° N~50° N, with cyclones over northeast Asia (110°~120°, 40° N) and central North Pacific (160°~180°, 45°

N), and an anticyclone over the American northwest (240° , 55° N). In the present study, the northern hemispheric branch of the Rossby wave pair, as well as the cyclone over northeast Asia, contribute to the anomalous low- V_s pocket observed south of Japan.

The result found here for Typhoon Soudelor, that both Z_{26} and V_s may contribute to the storm's intensity change, including rapid intensity change, has previously been noted in other studies that examine environmental influences. We highlight two such studies here, for Hurricane Opal (1–5 October 1995) in the Gulf of Mexico and Typhoon Maemi (6–13 September 2003) in the Philippine Sea. Shay et al. [15] noted that Opal rapidly intensified as it passed over a Loop Current eddy, where Z_{26} is generally deep, 50–100 m (for example, see [36]). However, the environmental attribution of intensification to the deep Z_{26} alone may not be complete. Bozart et al. [37] found that Opal's rapid intensification coincided also with when the environmental vertical wind shear dropped below 4 m/s. In Maemi's case, Lin et al. [7] associated its rapid intensification with when the storm crossed a warm ocean eddy (defined as "WOE-2" in [7]), where Z_{26} was deep, ≈ 70 m. The authors cautioned however that the simultaneous influence of a weak environmental vertical wind shear might also have contributed to the storm's intensification. We plot in Figure 9 the pre-Maemi (1 September 2003) large-scale vertical wind shear from the NCEP data to represent the storm's environmental vertical wind shear, and overlay the storm track as well as the location of the WOE-2. Several pockets of low $V_s < 4$ m/s are found in the plot, and Maemi's rapid intensification period can be seen to coincide with when the storm entered and exited one such pocket east of the Luzon Strait, where the WOE-2 was also located. In these as well as other cases, it would not be possible to unambiguously associate Z_{26} and/or V_s with the intensity change (assuming such an association exists). A better appreciation of the influences of Z_{26} and V_s on intensity change may be gained by conducting a more detailed attribution analysis, perhaps using a method similar to the one described herein for Typhoon Soudelor.

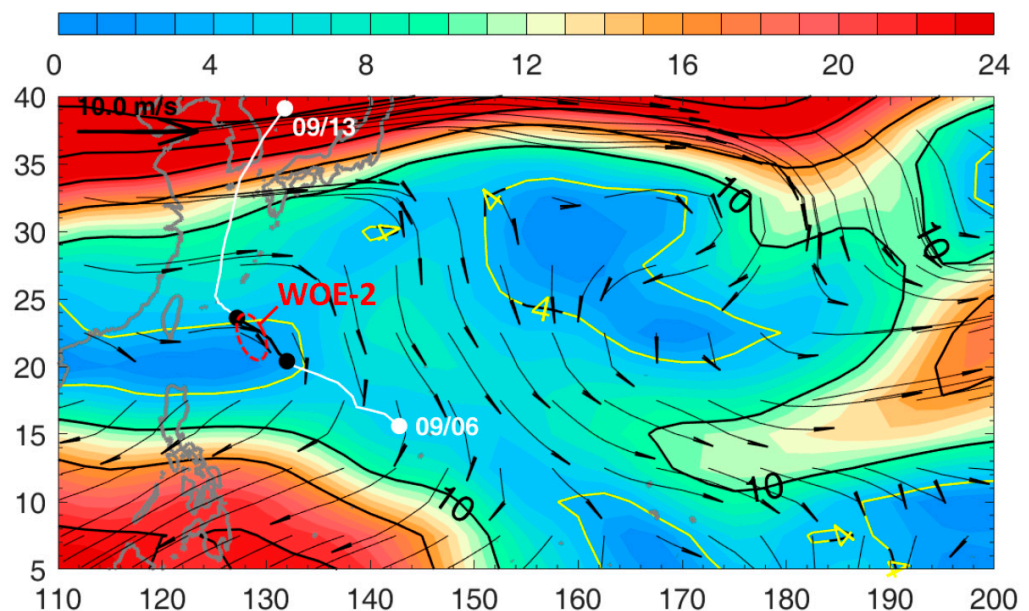


Figure 9. Pre-Typhoon Maemi (1 September 2003) vertical wind shear, $V_{200\text{hPa}} - V_{850\text{hPa}}$, and magnitude, $V_s = |V_{200\text{hPa}} - V_{850\text{hPa}}|$, V = wind velocity: vectors and color shading with contours = 4, 10, 16, etc., $m\ s^{-1}$, the 4 m/s contour is highlighted in yellow, calculated from the NCEP reanalysis data. Maemi track (6–13 September UTC) is shown and black line and markers indicate the rapid intensification period (Sep/08/12:00–Sep/10/00:00 UTC) as the storm entered and exited a “pocket” of weak wind shear enclosed by the 4 m/s contour east of the Luzon Strait. The warm ocean eddy “WOE-2” (from [7]) is indicated in red.

Finally, it is worth noting that in all three cases—Typhoon Soudelor, Hurricane Opal and Typhoon Maemi—rapid intensifications coincide with where the environmental vertical wind shear drops below 4 m/s, in agreement with Paterson et al. [8].

5. Conclusions

This paper uses observations to examine the environmental influences on the intensity change of Typhoon Soudelor in the western North Pacific. Due to the relatively small features of the ocean's 26 °C isotherm depth (Z_{26}) and the environmental vertical wind shear (V_s), with scales of 200~500 km and 500~1500 km, respectively, Soudelor's intensity change may be correlated with the varying Z_{26} and V_s environments as the storm crosses them. We found that Typhoon Soudelor's rapid intensification and weakening coincided with when the storm entered and left a pocket of low $V_s < 4$ m/s. A regression analysis indicated that the environmental influence to intensity change by V_s was largest (62%), followed by Z_{26} (27%) and others. On the other hand, Soudelor's subsequent weakening correlated well with decreasing background Z_{26} , as the storm moved further north. A composite analysis indicated that the low- V_s pocket was a consistent feature of the atmospheric condition in the western North Pacific in the summer preceding a strong El Nino, and that it was most likely forced by the northern hemispheric branch of the Matsuno-Gill's Rossby wave pair in response to tropical heating by El Nino.

Author Contributions: L.O. wrote the paper. Both L.O. and Y.L. conducted the data analyses and prepared the graphics. All authors have read and agreed to the published version of the manuscript.

Funding: This research was funded by the Ministry of Science and Technology of Taiwan, grant numbers 107-2111-M-008-035 and 107-2611-M-008-003.

Institutional Review Board Statement: Not applicable.

Informed Consent Statement: Not applicable.

Data Availability Statement: The data presented in this study are openly available from IBTrACS, EN4, Argo, AVISO, GHRSSST, and NCEP.

Acknowledgments: We thank the three reviewers whose comments improved the manuscript.

Conflicts of Interest: The authors declare no conflict of interest. The funders had no role in the design of the study; in the collection, analyses, or interpretation of data; in the writing of the manuscript, or in the decision to publish the results.

References

1. Gray, W.M. *Tropical Cyclone Genesis*; Report, No. CSU-ATSP-234; Dept. Atmos Sci Colorado State University: Fort Collins, CO, USA, 1975; 121p.
2. Emanuel, K.A. An air-sea interaction theory for tropical cyclones. Part I: Steady-state maintenance. *J. Atmos. Sci.* **1986**, *43*, 585–605. [[CrossRef](#)]
3. Bister, M.; Emanuel, K.A. Dissipative heating and hurricane intensity. *Meteorol. Atmos. Phys.* **1998**, *65*, 233–240. [[CrossRef](#)]
4. Gray, W.M. The formation of tropical cyclones. *Meteor. Atmos. Phys.* **1998**, *67*, 37–69. [[CrossRef](#)]
5. Gray, W.M. Global view of the origin of tropical disturbances and storms. *Mon. Wea. Rev.* **1968**, *96*, 669–700. [[CrossRef](#)]
6. Zehr, R.M. Environmental vertical wind shear with Hurricane Bertha. *Wea. Forecast.* **2003**, *18*, 345–356. [[CrossRef](#)]
7. Lin, I.I.; Wu, C.C.; Emanuel, K.; Lee, I.H.; Wu, C.R.; Pun, I.F. The interaction of Supertyphoon Maemi (2003) with a warm ocean eddy. *Mon. Weather Rev.* **2005**, 2635–2649. [[CrossRef](#)]
8. Paterson, L.A.; Hanstrum, B.N.; Davidson, N.E.; Weber, H.C. Influence of Environmental Vertical Wind Shear on the Intensity of Hurricane-Strength Tropical Cyclones in the Australian Region. *Mon Weather Rev.* **2005**, *133*, 3644–3660. [[CrossRef](#)]
9. Zeng, Z.; Wang, Y.; Wu, C.C. Environmental dynamical control of tropical cyclone intensity—An observational study. *Mon. Weather Rev.* **2007**, *135*, 38–59. [[CrossRef](#)]
10. Mainelli, M.; DeMaria, M.; Shay, L.K.; Goni, G. Application of oceanic heat content estimation to operational forecasting of recent Atlantic category 5 hurricanes. *Weather Forecast.* **2008**, *23*, 3–16. [[CrossRef](#)]
11. Hendricks, E.A.; Peng, M.S.; Fu, B.; Li, T. Quantifying environmental control on tropical cyclone intensity change. *Mon. Weather Rev.* **2010**, *138*, 3243–3271. [[CrossRef](#)]
12. Chen, X.; Wang, Y.; Zhao, K. Synoptic flow patterns and large-scale characteristics associated with rapidly intensifying tropical cyclones in the South China Sea. *Mon. Weather Rev.* **2015**, *143*, 64–87. [[CrossRef](#)]

13. Sun, J.; Oey, L.; Xu, F.; Lin, Y.C. Sea level rise, surface warming, and the weakened buffering ability of South China Sea to strong typhoons in recent decades. *Nature Sci. Rep.* **2017**, *7*, 7418. [[CrossRef](#)] [[PubMed](#)]
14. Balaguru, K.; Foltz, G.R.; Leung, L.R.; Hagos, S.M.; Judi, D.R. On the use of ocean dynamic temperature for hurricane intensity forecasting. *Weather Forecast.* **2018**, *33*, 411–418. [[CrossRef](#)]
15. Shay, L.K.; Goni, G.J.; Black, P.G. Effects of a warm oceanic feature on Hurricane Opal. *Mon. Weather Rev.* **2000**, *128*, 1366–1383. [[CrossRef](#)]
16. Chang, Y.L.; Oey, L.Y. Interannual and seasonal variations of Kuroshio transport east of Taiwan inferred from 29 years of tide-gauge data. *Geophys. Res. Lett.* **2011**, *38*, L08603. [[CrossRef](#)]
17. Chang, Y.L.; Oey, L.Y. The Philippines–Taiwan Oscillation: Monsoon like interannual oscillation of the subtropical–tropical western North Pacific wind system and its impact on the ocean. *J. Climate* **2012**, *25*, 1597–1618. [[CrossRef](#)]
18. Chelton, D.B.; Schlax, M.G.; Samelson, R.M. Global observations of nonlinear mesoscale eddies. *Prog. Oceanogr.* **2011**, *91*, 167–216. [[CrossRef](#)]
19. Good, S.A.; Martin, M.J.; Rayner, N.A. EN4: Quality controlled ocean temperature and salinity profiles and monthly objective analyses with uncertainty estimates. *J. Geophys. Res. Oceans* **2013**, *118*, 6704–6716. [[CrossRef](#)]
20. Sun, J.; Oey, L.Y. The influence of ocean on Typhoon Nuri (2008). *Mon. Weather Rev.* **2015**, *143*, 4493–4513. [[CrossRef](#)]
21. Emanuel, K.A. Environmental factors affecting tropical cyclone power dissipation. *J. Clim.* **2007**, *20*, 5497–5509. [[CrossRef](#)]
22. Camargo, S.J.; Sobel, A.H.; Barnston, A.; Emanuel, K. Tropical cyclone genesis potential index in climate models. *Tellus* **2007**, *59A*, 428–443. [[CrossRef](#)]
23. Price, J.F. Metrics of hurricane–ocean interaction: Vertically-integrated or vertically-averaged ocean temperature? *Ocean Sci.* **2009**, *5*, 351–368. [[CrossRef](#)]
24. Kobashi, F.; Kubokawa, A. Review on North Pacific subtropical countercurrent and subtropical fronts: Role of mode waters in ocean circulation and climate. *J. Oceanogr.* **2012**, *68*, 21–43. [[CrossRef](#)]
25. Liang, A.; Oey, L.; Huang, S.; Chou, S. Long-term trends of typhoon-induced rainfall over Taiwan: In situ evidence of poleward shift of typhoons in western North Pacific in recent decades. *J. Geophys. Res. Atmos.* **2017**, *122*. [[CrossRef](#)]
26. Kaplan, J.; DeMaria, M. Large-scale characteristics of rapidly intensifying tropical cyclones in the North Atlantic basin. *Weather Forecast.* **2003**, *18*, 1093–1108. [[CrossRef](#)]
27. Li, D.Y.; Huang, C.Y. The influence of ocean on intensity of Typhoon Soudelor (2015) as revealed by coupled modeling. *Atmos. Sci. Lett.* **2019**, *20*, 1–7. [[CrossRef](#)]
28. Press, W.H.; Teukolsky, S.A.; Vetterling, W.T.; Flannery, B.P. *Numerical Recipes*, 2nd ed.; Cambridge Univ. Press: New York, NY, USA, 1992; 933p.
29. Frank, W.M.; Ritchie, E.A. Effects of vertical wind shear on the intensity and structure of numerically simulated hurricanes. *Mon. Weather Rev.* **2001**, *129*, 2249–2269. [[CrossRef](#)]
30. Krishnamurti, T.N. Tropical east-west circulation during the northern summer. *J. Atmos. Sci.* **1971**, *28*, 1342–1347. [[CrossRef](#)]
31. White, G.H. An observational study of the Northern Hemisphere extratropical summer general circulation. *J. Atmos. Sci.* **1982**, *39*, 24–40. [[CrossRef](#)]
32. L’Heureux, M.L.; Takahashi, K.; Watkins, A.B.; Barnston, A.G.; Becker, E.J.; di Liberto, T.E.; Gamble, F.; Gottschalck, J.; Halpert, M.S.; Huang, B.; et al. Observing and predicting the 2015/2016 El Niño. *BAMS* **2017**, *7*, 1363–1382. [[CrossRef](#)]
33. Wen, N.; Li, L.; Luo, J.J. Direct impacts of different types of El Niño in developing summer on East Asian precipitation. *Clim Dyn.* **2020**, *55*, 1087–1104. [[CrossRef](#)]
34. Matsuno, T. Quasi-geostrophic motions in the equatorial area. *J. Meteorol. Soc. Jpn.* **1966**, *44*, 25–43. [[CrossRef](#)]
35. Gill, A.E. Some simple solutions for heat-induced tropical circulation. *Quart. J. Roy. Meteor. Soc.* **1980**, *106*, 447–462. [[CrossRef](#)]
36. Oey, L.-Y.; Ezer, T.; Lee, H.C. Loop Current, rings and related circulation in the Gulf of Mexico: A review of numerical models and future challenges. In *Circulation in the Gulf of Mexico: Observations and Models*; Sturges, W., Lugo-Fernandez, A., Eds.; American Geophysical Union: Washington, DC, USA, 2005; Volume 161, pp. 31–56.
37. Bozart, L.E.; Velden, C.S.; Bracken, W.D.; Molinari, J.; Black, P.G. Environmental influences on the rapid intensification of Hurricane Opal (1995) over the Gulf of Mexico. *Mon. Weather Rev.* **2000**, *128*, 322–352. [[CrossRef](#)]